Nonlinear deformation and progressive failure of multiwalled carbon nanotubes under internal radial pressure

J. R. Xiao[1] and J. W. Gillespie, Jr.[1,2,3]
[1]*University of Delaware Center for Composite Materials (UD-CCM), Newark, Delaware 19716, USA*
[2]*Department of Materials Science and Engineering, University of Delaware, Newark, Delaware 19716, USA*
[3]*Department of Civil and Environmental Engineering, University of Delaware, Newark, Delaware 19716, USA*
(Received 28 October 2005; revised manuscript received 17 July 2006; published 4 October 2006)

An analytical molecular structural mechanics model has been developed for the nonlinear deformation of multiwalled carbon nanotubes (MWCNTs) under internal radial pressure. Two sources of nonlinearity (i.e., nonlinear in-plane behavior of tube walls and nonlinear van der Waals interactions between layers) are considered. The nonlinear in-plane hoop force resultant-strain relationships of nanotube layers have been derived based on the modified Morse potential, and nonlinear van der Waals interaction has been considered by using the universal graphite potential. Two sets of Morse potential parameters are examined, the effect of van der Waals forces on load transfer between layers in MWCNTs are studied, and the ultimate pressure capacities of MWCNTs under internal pressure have been predicted based on a progressive failure analysis.

DOI: 10.1103/PhysRevB.74.155404 PACS number(s): 61.46.−w, 81.07.De

Carbon nanotubes[1–5] are a promising material for new composite materials, technologies, and devices. Of particular interest are their applications as nanofluidic devices.[6–9] multiwalled carbon nanotubes (MWCNTs) are expected to have higher radial stiffness and pressure resistance than single-walled carbon nanotubes (SWCNTs)[10] since they consist of multiple cylindrical layers held together by van der Waals forces. Theoretical investigation of the stress/strain state of MWCNTs subjected to internal pressure at infinitesimal strain has been conducted by Galanov *et al.*[9] This study was limited to the prediction of the stress/strain distribution in different layers using two proposed models with constant in-plane properties and constant van der Waals stiffness assumed. When MWCNTs are subjected to internal radial pressure acting on their innermost layer, the load will transfer among layers through the weak van der Waals interaction between layers. The interaction and displacement of each layer are different and dependent on its hoop stiffness and radius. As we know, the hoop stiffness of a SWCNT is size-dependent and the radial resistance of a single layer shows even more dependence on their geometry.[10] Furthermore, both the hoop stiffness[10] and the van der Waals interaction[11,12] are not constant when MWCNTs undergo large radial deformation. Hence, to predict the ultimate strength and failure of MWCNTs under internal pressure, both nonlinear in-plane behavior and nonlinear van der Waals interactions must be included in the analysis.

The van der Waals interactions are often modeled using the general Lennard-Jones "6-12" potential.[13] Since we are interested in MWCNTS with large innermost diameter (>2 nm), the interlayer interaction potential between any two adjacent tubes can be approximated by the universal graphite potential[12] obtained for two flat graphene sheets by assuming a continuous distribution of atoms on the tube surfaces and integrating the LJ carbon-carbon potential centered on atomic sites. The nonlinear stiffness $c(R)$ of van der Waals interaction between layers can be found in Ref. 11 [Eq. (40)] as a function of distance between two adjacent tubes.

Recent developments based on continuum or molecular mechanics have been reported for estimating elastic properties of nanotubes.[11,14–21] Among them, the authors of Ref. 11 as well as other researchers[16,17] have used the harmonic energy potential for the C-C bond to give constant in-plane stiffness, which is only valid for infinitesimal deformation. When a nanotube is subjected to external pressure,[11] the nanotube wall is under in-plane compression. It is known that under compression, tube failure occurs by buckling at small strains. Hence the harmonic potential with force constants is sufficient for the impulsive interaction of the C-C bond. In contrast, MWCNTs under internal radial pressure generate in-plane tension in the tube walls, which are capable of sustaining large deformation in this load scenario. In order to model the mechanical behavior of nanotubes up to or beyond bond breaking due to tension, a more complex interatomic potential function has to be used. The authors of Ref. 18 have extended the analytical molecular mechanics model[17] by incorporating the modified Morse potential function[22] to estimate elastic constants and stress-strain relationships of SWCNTs under tensile and torsional loadings. The predicted stress-strain relationships agree well with MD results[22] of SWCNTs under axial tension. This analytical molecular mechanics model can be easily modified to analyze the tensile behavior of SWCNTs in the hoop direction.

The present study aims to develop analytical methodologies based on molecular mechanics to quantify mechanical behavior (radial stiffness and pressure resistance) of MWCNTs under hydrostatic internal pressure with open ends. For each tube layer with tube diameter D, the radial displacement w is induced by hoop strain ε_θ defined by the strain-displacement relationship for an axisymmetric body (i.e., $w=D\varepsilon_\theta/2$). To calculate the hoop strain, the hoop force resultant, and the hoop surface, Young's modulus Y_θ of a nanotube must be predicted. The hoop force resultant S_θ (with units of N/m) under radial pressure p can be determined using Newton's first law of motion as $S_\theta=pD/2$. The hoop stiffness of the nanotube wall is calculated by the molecular structural mechanics model presented in Xiao *et al.*,[18]

where the relationship between hoop force resultant and bond stretch and bond angle variation can be determined through equilibrium and geometry of the nanotube structure by using a stick to model the force-stretch relationship of the C-C bond and a spiral spring to model the angle bending moment resulting from an angular variation of bond angle. The force-stretch relationship and the angle-variation moment relationship can be obtained from energy potential functions. With geometry information of bond connections,[18,23] one can obtain an equilibrium configuration at any loading level with the hoop force resultant (a uniform distributed force per unit length along the hoop direction in the average sense) and strain ε_θ in the nanotube. The modified Morse potential function[22] is used here. There are two sets of parameters for D_e and β given in Belytschko *et al.*[22] The first set of parameters (D_e=6.031 eV and β =26.25 nm^{-1}), denoted as M1, corresponds to the Brenner potential[21] for strain below 10% with a separation (dissociation) energy of 124 kcal/mol (5.62 eV/at), and the force field shape of this simple potential function is essentially the same as that of the Brenner potential function[24] before the inflection point (i.e., the maximum of the interatomic force). The second set of parameters (D_e=2.895 eV and β =38.43 nm^{-1}), denoted as M2, was proposed with a lower inflection point to consider defect formation due to mechanical strain. More detailed information about those parameters can be seen in Refs. 18 and 22.

Force resultant-strain relationships of armchair nanotubes can be obtained for both modified potential parameters (M1 and M2) up to the ultimate strength of nanotubes, which corresponds to the inflection point of C-C bond. M1 gives higher strength and failure strain of nanotubes than M2. It should be noted that force resultant-strain relationships for larger diameter SWCNTs (>2 nm) are similar and differences are negligible. The secant in-plane stiffness decreases as strain increases because of the nonlinear behavior of the tube walls.[18] Similar results can be obtained for zigzag tubes. It should be noted that in-plane stiffnesses are size-dependent when the tube diameter is less than 2 nm.

Uniform radial pressure provides an ideal condition to study the radial deformation of carbon nanotubes with open ends. For each layer, the relationship between the applied pressure and radial displacement w can be established as $P=(4Y_\theta/D^2)w$. Consequently, a radial stiffness can be defined as $Y_r=4Y_\theta/D^2$, which shows strong geometry dependence $(1/D^2)$ and rapidly decreases as the diameter increases. Due to the highly nonlinear nature (both the in-plane stiffness and the van der Waals force) of the problem of MWCNTs under internal pressure, we derive equations in incremental form and solve them by a displacement-controlled iterative method. Considering the equilibrium state of each layer, the following matrix system can be obtained:

$$\begin{bmatrix} \frac{Y_{\theta 1}}{r_1^2}+c & -c & & & \\ \cdots & \cdots & \cdots & \cdots & \cdots \\ & -\frac{r_{i-1}}{r_i}c & \frac{Y_{\theta i}}{r_i^2}+\left(\frac{r_{i-1}}{r_i}+1\right)c & -c & \\ \cdots & \cdots & \cdots & \cdots & \cdots \\ & & & -\frac{r_{n-1}}{r_n}c & \frac{Y_{\theta n}}{r_n^2}+\frac{r_{n-1}}{r_n}c \end{bmatrix} [\dot{\delta}]=[\dot{F}], \tag{1}$$

where $[\dot{F}]$ is the incremental loading vector $[\dot{F}]=[0\ 0\ \cdots\ 0\ \cdots\ 0\ \dot{P}]^T$ and $[\dot{\delta}]$ is the vector of incremental displacements of layers $[\dot{\delta}]=[\dot{w}_1\ \dot{w}_2\ \cdots\ \dot{w}_i\ \cdots\ \dot{w}_{(n-1)}\ \dot{w}_n]^T$, in which subscript 1 denotes the innermost layer and subscript n denotes the outermost layer of a MWCNT.

It can be seen that Eq. (1) looks similar to that of MWCNTs under external pressure[11] where only one nonlinearity arising from the van der Waals interaction was present. However, it should be noted that two sources of nonlinearity are involved in the present problem, where the secant in-plane stiffness $Y_{\theta i}$ of each layer is a function of $\varepsilon_{\theta i}$ and the van der Waals stiffness $c(R)$ is also a function of deformation [Eq. (40) in Ref. 11], where R is the distance between two neighboring tubes. The nonlinear equation can be solved by the Newton-Raphson method. A multistep procedure is performed at each iteration: (i) updating the in-plane stiffness of each layer by the analytical molecular mechanics model,[18] (ii) updating the van der Waals stiffness of each of two neighboring layers using Eq. (40) in Ref. 11, and (iii) solving Eq. (1) by the consecutive elimination of unknowns beginning with the first equation.

In the present study, the radial deformation of the 30-layer MWCNT[9] with an innermost radius of 30 nm under internal pressure is first studied with particular focus on their nonlinear deformation due to both the nonlinear van der Waals interaction and the nonlinear in-plane behavior of each layer, which is followed by results for the radial behavior of MWCNTs with different innermost diameters and layer numbers.

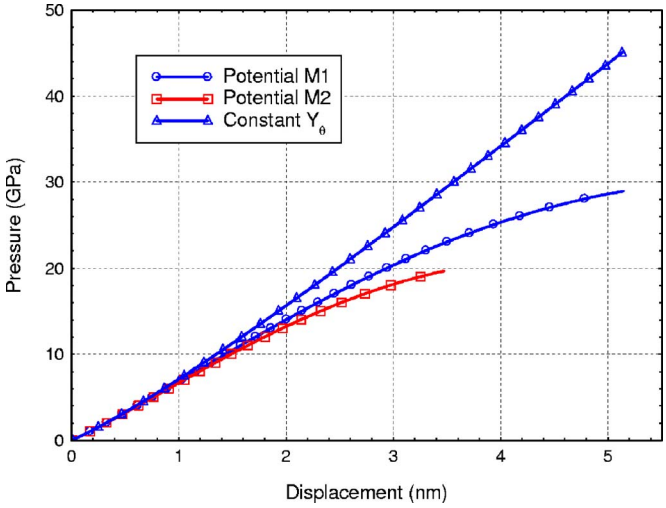

FIG. 1. (Color online) Effect of nonlinear van der Waals stiffness on pressure-displacement relationships of the 30-layer MWCNT under internal pressure prior to yield.

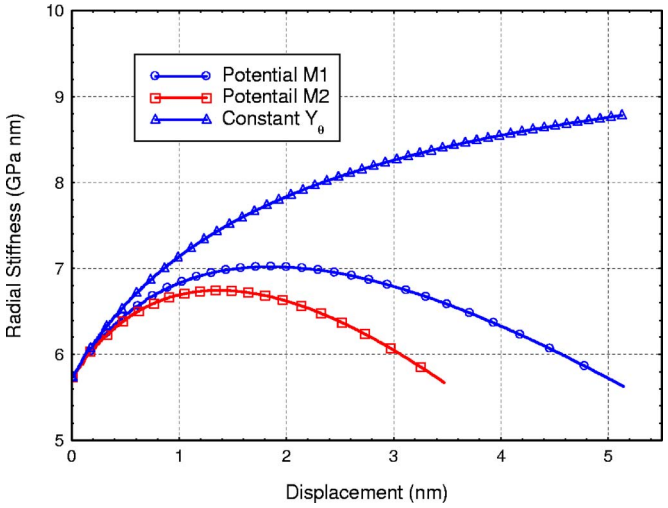

FIG. 2. (Color online) Nonlinear radial stiffness-displacement relationship of the 30-layer MWCNT under internal pressure prior to yield.

The 30-layer MWCNT is assumed to be made of armchair nanotubes with an interlayer distance of 0.341 nm. Figure 1 gives pressure displacements of the 30-layer MWCNT under nonlinear van der Waals interaction assumptions in which three different potential functions (harmonic, Morse potentials M1 and M2) are examined. The displacements are taken from the innermost layer of the MWCNT. The calculations are stopped at the inflection point of the C-C bond (Morse potentials M1 and M2), which corresponds to failure of the innermost layer. The results based on the harmonic potential (constant in-plane stiffness) are stopped at the same strain level as M1 for comparison purposes only. As discussed above, the harmonic potential is not suitable to the present load scenario. It can be seen that the harmonic potential gives a concave nonlinear pressure-displacement relationship because the van der Waals stiffness increases as the relative displacement of two neighboring tubes decrease. In contrast, M1 and M2 give concave responses up to a displacement of 1.5 nm, and the curves become convex as the displacement increases. The M2 potential has lower pressure capacity and failure displacement than the M1 potential. For instance, M1 and M2 give pressure capacities of 28.9 and 19.7 GPa, which are much lower than 45.0 and 29.2 GPa with constant Y_θ at the same displacement (corresponding to the inflection point) of M1 and M2, respectively. Clearly, the harmonic potential overestimates the pressure capacity at larger deformation since the harmonic potential is valid only for small deformation. Figure 2 shows the effect of van der Waals interactions and nonlinear in-plane stiffness on radial stiffness as the pressure increases. With constant Y_θ, the radial stiffness increases monotonically as deformation increases, and this increase is attributed to the nonlinear van der Waals interaction only. If the two sources of nonlinearity are considered, the radial stiffness increases up to a certain displacement then decreases as the displacement continues to increase.

Interlayer van der Waals forces at each layer of the 30-layer MWCNT at two different deformation levels (1.5 and 3.0 nm displacements) are shown in Fig. 3 to better understand the mechanisms of how MWCNTs resist radial pressure and how the loading is transferred between layers. It can be seen that the van der Waals force decreases from the innermost to the outermost layer. The jump at each layer indicates the radial resistance of each single tube. The difference between any two adjacent layers is due to the effect of their different circumferences. Such effects are not significant for larger diameters.

The pressure-displacement relationships of selected layers (layer 1, 10, 20, and 30) of the 30-layer MWCNTs are shown in Fig. 4, in which only results of M1 are presented. It can be seen that the largest radial deformation occurs at the innermost layers and the radial deformation decreases from the innermost layer to the outer layers at all pressure levels.

The failure mechanism of MWCNTs presents a complex problem that has not been well studied. However, there are a number of theoretical studies on the failure of SWCNTs that

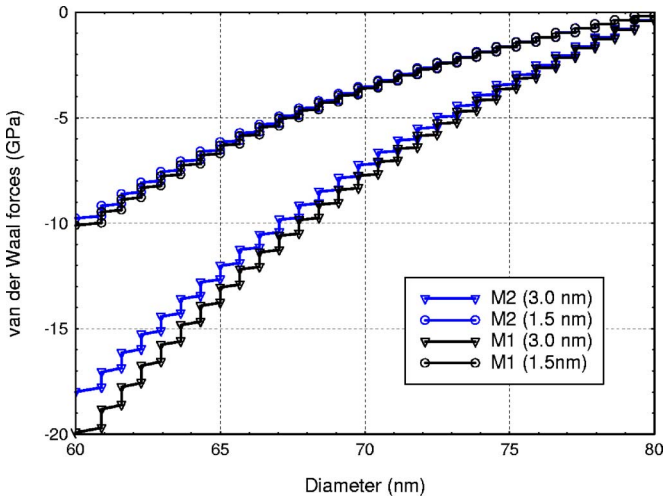

FIG. 3. (Color online) Van der Waals radial interaction and load transfer along layers of MWCNT under internal pressure at different deformation levels prior to yield.

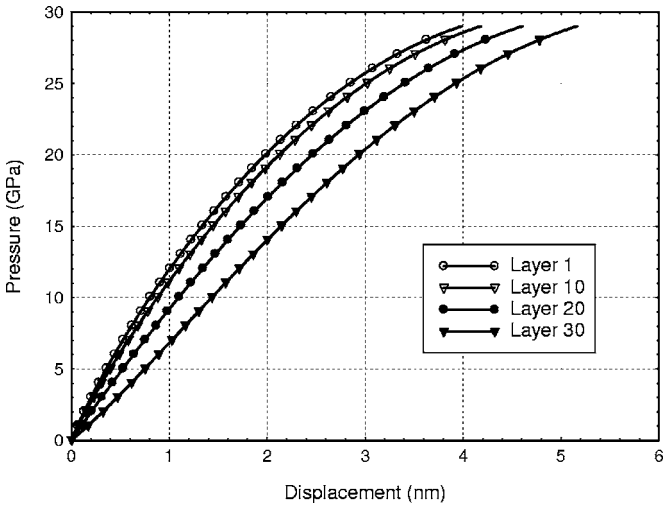

FIG. 4. Nonlinear radial pressure-displacement curves of the interlayer of the 30-layer MWCNT under internal pressure.

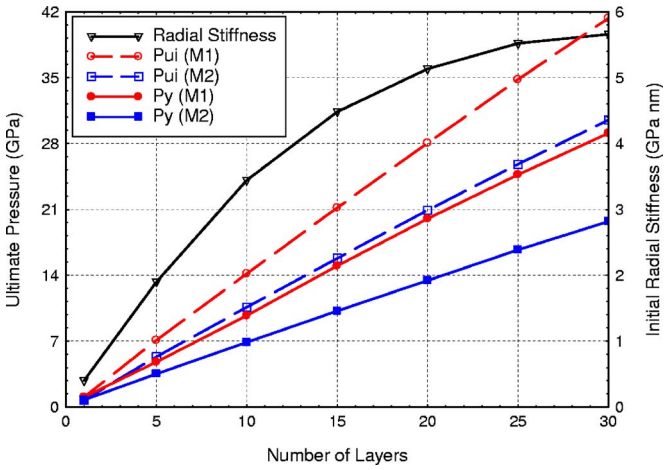

FIG. 5. (Color online) Initial radial stiffness and ultimate internal pressure of MWCNTs with different number of layers (same innermost diameter).

have been carried out using both classical and quantum MD simulations.[25–29] The foremost belief is that the failure of nanotubes is affected by the formation of pentagon/heptagon defects (the Stone-Wales bond rotation[30]). The 5-7-7-5 defect is initially formed, and for certain types of SWCNTs and at sufficiently high temperature it can lead to plastic yielding where the "5-7-7-5" dislocation evolves as a couple of dislocations gliding away along the spiral slip plane. Nardelli *et al.*[28] studied the mechanism of strain release under tension and they found that topological defects such as the 5-7-7-5 defect tend to form when strain is greater than 5% in order to achieve the relaxation of the structure. The atomistic-based continuum mechanics model[15] also predicted a similar critical Stone-Wales transformation strain of 5%. Nardelli *et al.*[29] observed the ductile-to-brittle failure transition as a function of both temperature and strain in their MD simulation. Generally, the failure modes fall into two different types: high strain (15%) and low temperature (1300 K) lead to brittle behavior (crack extension or propagation), while low strain (3%) and high temperature (3000 K) make nanotubes more ductile (dislocation motion without cracking).

The above studies were conducted for SWCNTs under axial tensile loading conditions. The authors assume the above two types of failure phenomena also exist in each individual layer of MWCNTs under internal pressure, which may lead to different failure scenarios. When a critical strain is reached and defects are initiated, under certain conditions (high temperature) ductile/dislocation-type failure (defect evolution and propagation) may occur (starting from the innermost layer) where a plateau stage of force/stress-strain relationship exists in each layer. Certainly the present approach is not able to deal with the high-temperature events. We limit our study on nanotubes under the high-strain/low-temperature regime (the effect of temperature is not considered explicitly). The brittle failure of nanotubes under axial tension has been evidenced by experiments[31] and MD simulations.[22,28] In this case, once the tube has failed (corresponding to the inflection point of a local broken bond), its loading capacity drops to zero immediately. The failure is localized.

However, in the case of MWCNTs under internal pressure, the failure patterns and evolutions may be different. The individual layer with local failure might sustain certain residual pressure that depends on the failure orientation. For simplicity, two bounding scenarios are assumed for considering the post-failure (after the inflection point) of nanotubes under internal pressure. The lower bound assumes the loading capacity drops to zero immediately once the force reaches its inflection point. The upper bound assumes the loading capacity remains constant at the failure level (defined at the inflection point). A third scenario is an intermediate response that follows the Morse potential beyond the inflection point and gradually drops to zero. These associated force fields with softening postpeak behavior (lower bound, upper bound, and intermediate response) are not intended for general applications, but are used here strictly to show the impact of progressive failure in MWCNTs.

Based on the lower bound assumption, once the innermost tube fails, the layer can be removed from the system from a mechanics point of view. The calculated pressure to fail the innermost layer of a 29-layer MWCNT (NT2) with the same outermost diameter as that of the 30-layer MWCNT (NT1) is 19.1 GPa, which is smaller than 19.7 GPa. Clearly after the innermost layer of NT1 fails, the pressure capacity of the remaining MWCNT (NT2) drops. If one maintains the same pressure of $P_y = 19.7$ GPa, the remaining MWCNT (NT2) will fail catastrophically. The so-obtained pressure is defined as the yield pressure, which is the lower bound on the pressure capacity of MWCNT.

The following results for the lower bound response will depict the dependence of the initial radial stiffness and yield pressure of MWCNTs on the number of layers and the diameters of MWCNTs. Figure 5 shows the initial radial stiffness and yield pressure (P_y) decrease as the number of layers is reduced from thirty to one (with the same innermost diameter of 30 nm). There are different tendencies between the initial radial stiffness and yield pressures (solid lines) as shown in Fig. 5, in which yield pressures show almost a linear dependence on the number of layers for both M1 and M2, while the initial radial stiffness shows a nonlinear in-

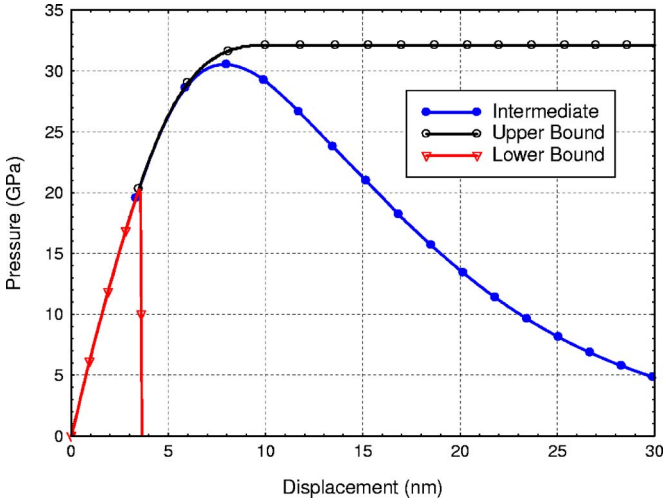

FIG. 6. (Color online) Nonlinear pressure-displacement curves of the innermost layer of MWCNTs with different post-failure behaviors (M2).

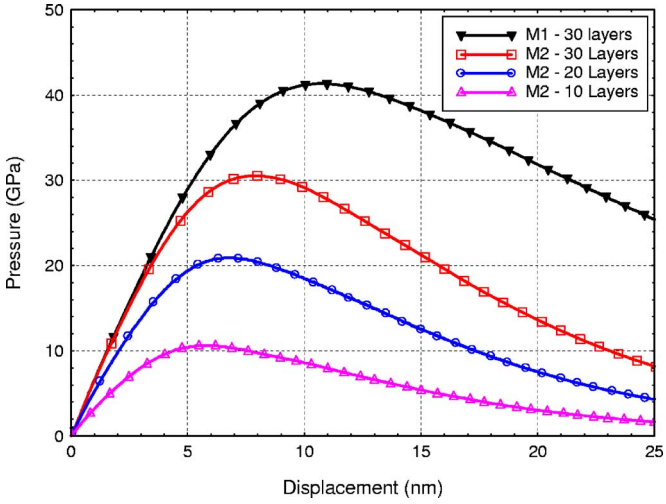

FIG. 7. (Color online) Nonlinear pressure-displacement curves of the innermost layer of MWCNTs with different number of layers (same innermost diameter; progressive failure with intermediate softening).

crease as the number of layers increases. To increase the initial radial stiffness and yield pressure of a MWCNT, one can imagine the "addition" of more outer layers into the MWCNT. However, it is noticed that, with a fixed innermost diameter, when the layers increase to a certain number, the initial radial stiffness becomes almost constant because of the weak van der Waals interaction between layers.

For the upper bound assumption, or any intermediate softening response, a progressive failure can be seen in the MWCNT. A displacement controlled nonlinear analysis is performed to predict the progressive failure behaviors. The pressure-displacement relationship of the 30-layer MWCNT based on the upper bound assumption is shown in Fig. 6, where the lower bound result is also indicated. The displacement is taken from the innermost layer of the MWCNT. It can be seen that the so-predicted ultimate pressure (32.3 GPa) is about 60% higher than the lower bound result (19.7), and the MWCNT can sustain constant pressure as displacement increases (until the layers are completely broken).

The above calculation based on the lower bound assumption may underestimate the ultimate pressure capability of a MWCNT if the failed layer(s) is able to carry some residual pressure. On the other hand, the calculation based on the upper bound assumption may overestimate the ultimate pressure capability of a MWCNT and give unrealistic post-failure response (constant pressure) as shown in Fig. 6. An intermediate softening response is expected to give more realistic response of a MWCNT. How to quantify the softening behavior remains an open issue. In the present study, we consider a softening response that follows the Morse potential beyond the inflection point as one possibility. The 30-layer MWCNT was analyzed again with M2 and the pressure-displacement relationship is shown in Fig. 6 for comparison. One can see that the pressures go beyond the yield pressures up to the ultimate values of 30.5 GPa, then the pressure decreases as displacement increases, which falls between two bounds. It is interesting to find that there is very little difference between the predicted ultimate pressures based on the intermediate response (the Morse potential), denoted as P_{ui}, and the upper bound result, denoted as P_u. If one increases the degree of post-failure softening behavior (correlating to lower separation energy), a lower ultimate pressure would be obtained (falling between our bounds). The displacements at failure (M2) are 3.64, 7.88, and 9.21 nm for lower bound, intermediate, and upper bound assumptions, respectively.

It should be noted that all layers reached their inflection point in the case of upper bound assumption. However, the outermost layer has not reached its inflection point at the ultimate pressure for the intermediate response, as shown in Fig. 6. We further reduced the number of layers and performed the progressive analyses on MWCNTs (same innermost radius) with 25, 20, 15, 10, and 5 layers. The pressure-displacement relationships (based on M2) of the 20- and 10-layer MWCNTs are presented in Fig. 7 and compared with those of the 30-layer MWCNT based on M1 (solid triangles) and M2 (open squares). The displacement was again taken from the innermost layer of MWCNTs. The calculated ultimate pressures (P_{ui}) with different layers (thickness) are also summarized in Fig. 5 (dashed lines). One can see that the ultimate pressures are higher than the corresponding yield pressures (same for the single-walled tube) and the ultimate pressure shows a linear dependence on the number of layers

TABLE I. Impact of progressive failure on ultimate pressure of MWCNTs (M2).

Total layers (innermost radius 30 nm)	30	25	20	15	10	5
$\frac{P_{ui}}{P_y}$	1.54	1.54	1.54	1.53	1.52	1.50
$\frac{P_u}{P_y}$	1.64	1.62	1.61	1.60	1.57	1.53

TABLE II. Yield layers of MWCNTs under ultimate pressure.

Total layers (same innermost radius 30 nm)	30	25	20	15	10	5
Yield layers (M1)	16	14	11	8	6	4
Yield layers (M2)	17	15	12	9	7	5
Innermost radius (nm) (30 layers)	30	60	90	120	150	180
Yield layers (M2)	17	19	21	23	26	30

for both M1 and M2. The ratios of P_{ui}/P_y and P_u/P_y based on M2 are presented in Table I to see the impact of the progressive failure on the ultimate pressure of MWCNTS with different layers.

The number of yield layers of the intermediate response is counted from each calculation and presented in Table II. It can be seen that as the layer number (same innermost diameter) decreases to five (thin tube), all the layers yield at the ultimate pressure. For thick tubes (for instance, larger than five layers with inner radius 30 nm), only partial tubes yield when the entire MWCNTs reach their ultimate pressures.

The effect of tube diameter on the yield and ultimate pressure capacity is presented in Fig. 8. The analyses are performed on six different MWCNTs with an innermost radius of 30, 60, 90, 120, 150, and 180 nm, respectively. It can be seen that both the yield and ultimate pressure decrease as their diameters increase. The yield layers based on M2 at each MWCNT were also counted and given in Table II. It can be seen that as the diameter increases, the number of yield layers increases and all layers yield in the MWCNT with an innermost radius of 180 nm. Generally, for a given MWCNT, its yield pressure depends on the inflection point of the potential and is independent of the separation energy, whereas the ultimate pressure and the number of layers yielding are determined by the post-failure behavior of each individual layer. In this study, it depends on the separation energy of the Morse potential, i.e., the force field after the inflection point. Higher separation energy gives higher ultimate pressure and more layers yield. For a given potential, whether the MWCNT is fully yielded (all layers) depends on both its diameter and the number of layers (thickness), as shown in Table II. If the individual layer loses its load capability completely at any conditions after the inflection point, the yield pressure is equivalent to the ultimate pressure.

It should be noted that the above results calculated using both M1 and M2 potentials give the same initial stiffness but different ultimate pressure capacities. M1 corresponds to defect-free tubes, and M2 was a modified potential[22] for considering defects (inherent or strain-induced). Defects may cause local damage or plastic deformation, and eventually, lead to failure at an earlier strain stage than that of defect-free CNTs. More investigations on the effect of defects will be conducted in future studies.

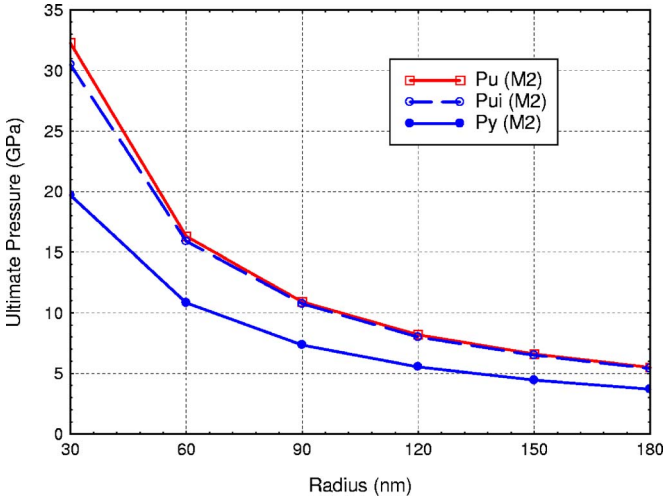

FIG. 8. (Color online) Ultimate internal pressure of 30-layer MWCNTs with different innermost radius.

In conclusion, an analytical progressive failure analysis methodology has been developed for the nonlinear deformation of MWCNTs (with open ends) under internal pressure. Two sources of nonlinearity were considered. Ultimate pressure has been predicted based on three different assumptions on the in-plane post-failure behavior of a single layer, i.e., lower bound, upper bound, and the intermediate response. The upper bound capacity is about 50–60 % higher than that of the lower bound (yield pressure) for thick tubes. The intermediate response gives an ultimate pressure between the two bounds, and the value depends on the softening phase. How to quantify the softening phase will be studied in the future. The yield pressure capacity is recommended as the operating pressure for nanofluidic devices, and the ultimate pressure resulting from progressive failure can be treated as a safety factor (P_u/P_y). This safety factor is not only affected by the in-plane softening phase of the tube wall, but also by the thickness (number of layers) of MWCNTs and their diameters.

[1] S. Iijima, Nature (London) **354**, 56 (1991).

[2] M. S. Dresselhaus, G. Dresselhaus, and P. C. Eklund, *Science of Fullerenes and Carbon Nanotubes* (Academic Press, San Diego, 1996).

[3] J. Che, T. Cagin, and W. A. Goddard, Nanotechnology **11**, 65 (2000).

[4] M. B. Nardelli, J. L. Fattebert, D. Orlikowski, C. Roland, Q. Zhao, and J. Bernholc, Carbon **38**, 1703 (2000).

[5] B. I. Yakobson and P. Avouris, in *Carbon Nanotubes*, edited by M. S. Dresselhaus, G. Dresselhaus, and P. Avouris, Topics in Applied Physics (Springer Verlag, Berlin, 2001), Vol. 80, pp. 287–329.

[6] M. A. Burns, B. N. Johnson, S. N. Brahmasandra, K. Handique, J. R. Webster, M. Krishnan, T. S. Sammarco, P. M. Man, D. Jones, D. Heldsinger, C. H. Mastrangelo, and D. T. Burke, Science **282**, 484 (1998).
[7] W. Schulz, Chem. Eng. News **2000**, 39–42 (2000).
[8] Y. Gogotsi, J. A. Libera, A. Guvenc-Yazicioglu, and C. M. Megaridis, Appl. Phys. Lett. **79**, 1021 (2001).
[9] B. A. Galanov, S. B. Galanov, and Y. Gogotsi, J. Nanopart. Res. **4**, 207 (2002).
[10] J. R. Xiao and J. W. Gillespie (unpublished).
[11] J. R. Xiao, S. L. Lopatnikov, B. A. Gama, and J. W. Gillespie, Mater. Sci. Eng., A **416**, 192 (2005).
[12] L. A. Girifalco, M. Hodak, and R. S. Lee, Phys. Rev. B **62**, 13104 (2000).
[13] J. E. Lennard-Jones, Proc. R. Soc. London, Ser. A **106**, 441 (1924).
[14] P. Zhang, Y. Huang, P. H. Geubelle, P. A. Klein, and K. C. Hwang, Int. J. Solids Struct. **39**, 3893 (2002).
[15] H. Jiang, P. Zhang, B. Liu, Y. Huang, P. H. Geubelle, H. Gao, and K. C. Hwang, Comput. Methods Appl. Mech. Eng. **193**, 3419 (2004).
[16] C. Y. Li and T. S. Chou, Int. J. Solids Struct. **40**, 2487 (2003).
[17] T. Chang and H. Gao, J. Mech. Phys. Solids **51**, 1059 (2003).
[18] J. R. Xiao, B. A. Gama, and J. W. Gillespie, Int. J. Solids Struct. **42**, 3075 (2005).
[19] T. Chang, J. Geng, and X. Guo, Appl. Phys. Lett. **87**, 251929 (2005).
[20] L. Shen and J. Li, Phys. Rev. B **69**, 045414 (2004).
[21] L. Shen and J. Li, Phys. Rev. B **71**, 035412 (2005).
[22] T. Belytschko, S. P. Xiao, G. C. Schatz, and R. Ruoff, Phys. Rev. B **65**, 235430 (2002).
[23] L. H. Ye, B. G. Liu, and D. S. Wang, Chin. Phys. Lett. **18**, 1496 (2001).
[24] D. W. Brenner, Phys. Rev. B **42**, 9458 (1990).
[25] B. I. Yakobson, M. P. Campbell, C. J. Brabec, and J. Bernholc, Comput. Mater. Sci. **8**, 341 (1997).
[26] B. I. Yakobson, in *Recent Advances in the Chemistry and Physics of Fullerenes and Related Materials*, edited by R. S. Ruoff and K. M. Kadish (Electrochemical Society, Pennington, NJ, 1997), pp. 549–560.
[27] M. B. Nardelli, B. I. Yakobson, and J. Bernholc, Phys. Rev. B **57**, R4277 (1998).
[28] M. B. Nardelli, B. I. Yakobson, and J. Bernholc, Phys. Rev. Lett. **81**, 4656 (1998).
[29] M. B. Nardelli, J.-L. Fattebert, D. Orlikowski, C. Roland, Q. Zhao, and J. Bernholc, Carbon **38**, 1703 (2000).
[30] A. J. Stone and D. J. Wales, Chem. Phys. Lett. **128**, 501 (1986).
[31] M. F. Yu, O. Lourie, M. J. Dyer, K. Moloni, T. F. Kelly, and R. S. Ruoff, Science **287**, 637 (2000).